Human Molecular Genetics, 2013, Vol. 22, No. 20 **4053–4063**
doi:10.1093/hmg/ddt255
Advance Access published on May 31, 2013

A mutation in *Tubb2b*, a human polymicrogyria gene, leads to lethality and abnormal cortical development in the mouse

R.W. Stottmann[1,2,3,†,*], M. Donlin[2], A. Hafner[4], A. Bernard[5], D.A. Sinclair[4] and D.R. Beier[1,‡]

[1]Division of Genetics, Department of Medicine, Brigham and Women's Hospital, Harvard Medical School, Boston, MA 02115, USA, [2]Division of Human Genetics and [3]Division of Developmental Biology, Cincinnati Children's Hospital Medical Center, Cincinnati, OH 45229, USA, [4]Paul F. Glenn Laboratories for the Biological Mechanisms of Aging, Department of Pathology/Genetics, Harvard Medical School, Boston, MA 02115, USA and [5]Allen Institute for Brain Science, Seattle, WA 98103, USA

Received March 18, 2013; Revised May 20, 2013; Accepted May 28, 2013

Human cortical malformations, including lissencephaly, polymicrogyria and other diseases of neurodevelopment, have been associated with mutations in microtubule subunits and microtubule-associated proteins. Here we report our cloning of the *brain dimple* (*brdp*) mouse mutation, which we recovered from an ENU screen for recessive perinatal phenotypes affecting neurodevelopment. We identify the causal mutation in the *tubulin, beta-2b* (*Tubb2b)* gene as a missense mutation at a highly conserved residue (N247S). *Brdp/brdp* homozygous mutants have significant thinning of the cortical epithelium, which is markedly more severe in the caudolateral portion of the telencephalon, and do not survive past birth. The cortical defects are largely due to a major increase in apoptosis and we note abnormal proliferation of the basal progenitors. Adult *brdp/+* mice are viable and fertile but exhibit behavioral phenotypes. This allele of *Tubb2b* represents the most severely affected mouse tubulin phenotype reported to date and this is the first report of a tubulin mutation affecting neuronal proliferation and survival.

INTRODUCTION

Mammalian cortical development requires precise regulation of a massive amount of cell division and migration. Neurons and glial cells must proliferate in very large numbers, migrate to appropriate positions in the cerebral cortex and extend multiple, and sometimes extremely long, cellular extensions. These processes involve mitosis, cell migration and neurite outgrowth, all requiring microtubules that consist of lengthy protofilaments composed of alternating α- and β-tubulin dimers. Defects in the function of microtubules and microtubule-associated proteins have been linked to an increasing number of human diseases, including cortical malformation syndromes (1). *Tubulin alpha-1A* (TUBA1A) is mutated in human patients with lissencephaly, pachygyria and polymicrogyria (2–7). Autosomal recessive mutations in *tubulin alpha-8* cause polymicrogyria with optic nerve hypoplasia (8). *Tubulin beta-3* (TUBB3) mutations have recently been identified in patients with a variety of disorders: the so-called TUBB3 syndromes. A series of heterozygous TUBB3 mutations results in ocular motility defects, agenesis of the corpus callosum (CC), anterior commissure dysgenesis and dysmorphic basal ganglia (9). Further mutations in TUBB3 have been found to cause cortical dysgenesis without associated deficits in extra-ocular musculature (10). Mutations in *tubulin beta-2b* (TUBB2B) were first identified in human patients with asymmetrical polymicrogyria (11). Other TUBB2B phenotypes noted were internal capsule hypoplasia, cerebellar atrophy, CC defects, disorganized cortical layering and disorganized radial glial scaffolds. Further studies have since found TUBB2B mutations in patients with a number of features which now overlap with other tubulin gene mutations and comprise a 'tubulinopathy-associated spectrum' (6). As a group, these disorders collectively feature neuronal migration defects, cerebellar hypoplasia, microcephaly, axon tract defects, seizures

*To whom correspondence should be addressed at: Tel: +1 5136367136; Fax: +1 5136364373; Email: rolf.stottmann@cchmc.org
†Present address: Divisions of Human Genetics and Developmental Biology, Cincinnati Children's Hospital Medical Center, Cincinnati, OH 45229, USA.
‡Present address: Center for Developmental Biology and Regenerative Medicine, Seattle Children's Research Institute, Seattle, WA 98105, USA.

Published by Oxford University Press 2013
This work is written by (a) US Government employee(s) and is in the public domain in the US.

Table 1. Summary of phenotypes from *Tubb2b* mutations to date in mice and humans

	G98R	L117P	G140A	S172P[a]	L207P	I210T	L228P	N247S	A248V	N256S	F265L	T312M	R380L	R380S	R380C	D417N	E421K
Polymicrogyria/neuronal migration defect	y	y	y	y	y	y	y	N/A	y	y	y	y	y	y	y	y	y
Basal ganglia affected	y	n	y	n	y	y	y	y	y	y	y	y	y	y	y	n	y
Cerebellar hypoplasia	y	n	y	N/A	y	y	y	y	y	n	y	y	y	y	y	n	N/R
Enlarged ventricles	y	N/R	y	N/R	y	N/R	N/R	y	y	N/R	N/R	N/R	y	y	y	n	N/R
Intellectual disability/deficits/delay	y	y	y	N/A	y	y	y	N/A	y	y	y	y	y	y	y	y	y
Small head circumference/microcephaly	y	y	y	N/A	y	y	y	N/A	y	y	y	y	y	y	y	y	y
Epilepsy/seizures	y	n	y	N/A	y	y	y	N/A	y	n	y	n	n	y	y	y	n
Reduced/absent CC	y	N/R	y	y	y	y	y	y	y	N/R	y	y	y	y	y	N/R	y
CFEOM/hypoplastic optic chiasm/optic atrophy	y	N/R	N/R	N/A	n	N/R	y	N/A	n	N/R	N/R	N/R	y	y	n	N/R	y
Ptosis	N/R	N/R	y	N/A	N/R	N/R	N/R	N/A	N/R	N/R	N/R	N/R	N/R	N/R	N/R	N/R	y
Mutant monomers incorporate into microtubules	N/R	N/R	N/R	n	N/R	y	y	y	N/R	N/R	n	y	N/R	N/R	N/R	N/R	y
Mutant monomers alter microtubule dynamics	N/R	N/R	N/R	y	N/R	n	n	n	N/R	N/R	y	n	N/R	N/R	N/R	N/R	y

N247S (our study); R380L, A248V (13); E421K (12); R380S, R380C, L207P, G98R (6); D417N, N256S, L117P (14); T312M, L228P, F265L, I210T, S172P (11); G140A (15).
CFEOM, congenital fibrosis of the extraocular muscles; y, yes; n, no; N/R, not reported. N/A, not applicable—this is noted for N247S to avoid confusion, as polymicrogryia cannot be scored in a mouse.
Our analysis did not indicate a block in neuronal migration (see Results).
[a]Mutation identified in fetus; many assays not able to be performed.

and optic tract defects (e.g. CFEOM: congenital fibrosis of the extraocular muscles; 6,11–15; Table 1). As these human genetic studies progress, phenotypes due to tubulin mutations in different genes are now beginning to overlap, consistent with a general requirement for microtubules in neurodevelopment with some distinct features for each tubulin gene. The human mutations identified to date are heterozygous, *de novo* mutations. The phenotypes of recessive tubulin mutations in the developing nervous system remain largely unknown.

The mouse is an informative model for human cortical development and some mouse alleles of tubulin genes have been characterized. The most commonly occurring human TUBB3 amino acid substitution has been engineered in a mouse model and the homozygotes have normal cortical layering but do have defects in axon guidance, including the CC, anterior commissure and cranial nerves (9). A *tubulin, beta1 class VI* (*Tubb1*) null allele has been reported with defects in platelet function (16). We have recently identified a novel mutation affecting cortical development as part of an ENU mutagenesis screen designed to ascertain neurodevelopmental phenotypes in the perinatal mouse embryo. Here we report on the *brain dimple* (*brdp)* mouse, a recessive mutant with multiple forebrain phenotypes, including a rather specific accumulation of intermediate progenitors. We also demonstrate an interesting and unexpected heterozygous behavioral phenotype in adult *brdp/+* heterozygous mice. We determined by positional cloning that *brdp* is due to a missense mutation in *tubulin, beta-2b* (*Tubb2b*). There is no genetic model of *Tubb2b*, but RNAi depletion in the rat has been shown to lead to neuronal migration defects. Our novel allele results in the most dramatic neurodevelopmental defect due to perturbation of β-tubulin function to date, suggesting that *Tubb2b* is a major isoform involved in cortical development.

RESULTS

Brain dimple mutants have severe defects in cortical development

We initially recovered the *brdp* mutation as part of an ENU mutagenesis screen designed to uncover novel recessive mutations necessary for normal cortical development (17). Upon initial dissection at embryonic day (E) 18.5, 1 day before birth, *brdp/brdp* homozygous mutants were largely normal, but can often be distinguished by their slightly shortened snouts (Fig. 1G). Dissection of the brain, however, revealed much more striking defects. Several structures in the mutant brains were severely reduced in size, including the olfactory bulbs, midbrain and cerebellum (Fig. 1H). The most dramatic defects were in the caudolateral telencephalon, where the thickness of the neuroepithelium is reduced in mutant tissue and the ventricles are significantly enlarged (Fig. 1H and I). At E18.5, we see no differences in the brain between *brdp/+* heterozygous mice (Fig. 1D–F) and wild-type controls (Fig. 1A–C).

Histological analysis of the *brdp/brdp* mutants confirmed an expansion of the ventricles and reduced neocortical epithelium in all regions, but most significantly in a caudo-lateral region roughly corresponding to the rhinencephalon (olfactory region; Fig. 2B, J and N). We also noted reduction in other structures of the brain, including the choroid plexus and the basal ganglia (Fig. 2B, H and J). Within the cerebral cortex, *brdp*

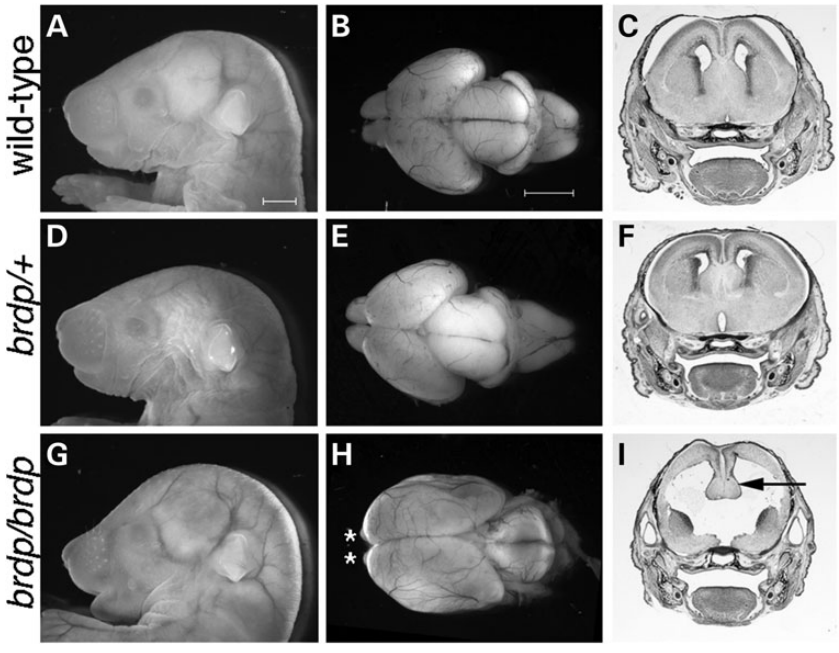

Figure 1. Brdp/brdp mutants have significant cortical malformations. (**A**, **D** and **G**) Wild-type, *brdp/+* and *brdp/brdp* embryos are indistinguishable upon initial dissection at E18.5 except for subtle craniofacial defects in the mutants. (**B**, **E** and **H**) Microdissection of the brain reveals significant phenotypes only in the *brdp/brdp* mutants including smaller olfactory bulbs (asterisks) and ventriculomegaly. Histological analysis (**C** and **F**) in the coronal plane shows no significant differences between wild-type and *brdp/+* mice. (**I**) The *brdp/brdp* mutant cortical neuroepithelium is thinner than wild-type and the reduction is most pronounced in the caudal and lateral cortices. Agenesis of the CC is also noted in the *brdp/brdp* mutants (arrow).

mutants have wave-like perturbations in the cortical plate (Fig. 2B, D and L) and a hypoplastic, irregular ventricular zone (VZ; Fig. 2D and F).

Most of the perinatal defects we see in *brdp/brdp* mutants at E18.5 were already present at E16.5. At this earlier stage, we noted thinning of the cortical neuroepithelium and hypoplastic basal ganglia (Fig. 3B). These defects are again more significant in posterior regions of the brain at E16.5 (Fig. 3D). At E14.5, the reduced basal ganglionic structures are evident with the defects again increasing in severity in the caudal portion of the cortex (Fig. 3F and H). Even at E11.5, at the onset of neurogenesis, the basal ganglia are slightly smaller in mutants compared with wild-types, although the overall patterning of the forebrain looks similar between *brdp* mutants and wild-type at this stage (Fig. 3I and J). A molecular analysis of the ganglionic eminences did not show profound patterning defects (Supplementary Material, Fig. S1). Progression of the patterning defect during postnatal development could not be evaluated, as *brdp/brdp* mutants do not survive past birth. The cause of this death has not been determined, but some P0 mutants were observed gasping, suggesting a respiratory control center has been disturbed. Taken together, all of these data suggest defects in neurogenesis particularly affecting the rhinencephalon, basal ganglia and the subventricular zone, which gives rise to the olfactory bulb. Our histological analysis also indicated that a number of fiber tracts are affected in the *brdp/brdp* homozygous mutant brain. We note agenesis of the CC, with associated Probst bundles, reduced striatal axons leading to and forming the internal capsule and loss of the anterior commissure (Figs 1I, 2B and 3B).

To further understand the *brdp/brdp* phenotype, we undertook a molecular analysis of the developing cortex in mutant and wild-type embryos. We first assayed neuroprogenitor proliferation rates in wild-type and *brdp/brdp* embryos by measuring phosphorylated histone H3 immunoreactivity (pHH3) (as a marker of M-phase) and calculating a mitotic index. Surprisingly, we saw an increased mitotic index in *brdp/brdp* mutants over control embryos at E14.5 (Fig. 4A–C; 143% increase in mutants, $P < 0.0001$). In addition to the increased mitotic index, we noted a number of pHH3 immunoreactive cells displaced away from the VZ in *brdp* mutants (Fig. 4B). This was quantified further and we note the number of pHH3 immunoreactive (and thus, mitotic) cells in the VZ is only modestly, but significantly, increased in mutants (Fig. 4D; 121%, $P = 0.025$). However, the cell divisions away from the VZ, corresponding to the IZ, are significantly increased (Fig. 4D; 388% increase, $P < 0.0001$). As a further measure of progenitor proliferation, we performed immunohistochemistry for phospho-vimentin and similarly saw increased immunoreactivity in *brdp/brdp* mutants (Fig. 4F). The increase in pHH3-positive cells away from the VZ suggests that intermediate progenitors may be affected in *brdp/brdp* mutants. We analyzed this with Tbr2 immunohistochemistry (Fig. 4G and H). We observed no significant increase in the number of Tbr2-positive progenitors at E12.5, but we did see a 16% increase at E14.5 (Fig. 4I; $P < 0.001$). We also used a TuJI antibody to label differentiated neurons in the cortical plate and see decreased TuJI expression in the *brdp/brdp* mutants when compared with wild-type (Fig. 4K). TuJI-expressing cells also occupied a broader portion of the developing cortex.

Radial glial cells are both a progenitor cell in the cortex and the scaffold for neuron migration at these stages. To assess morphology of radial glial cells as a potential source of the proliferation

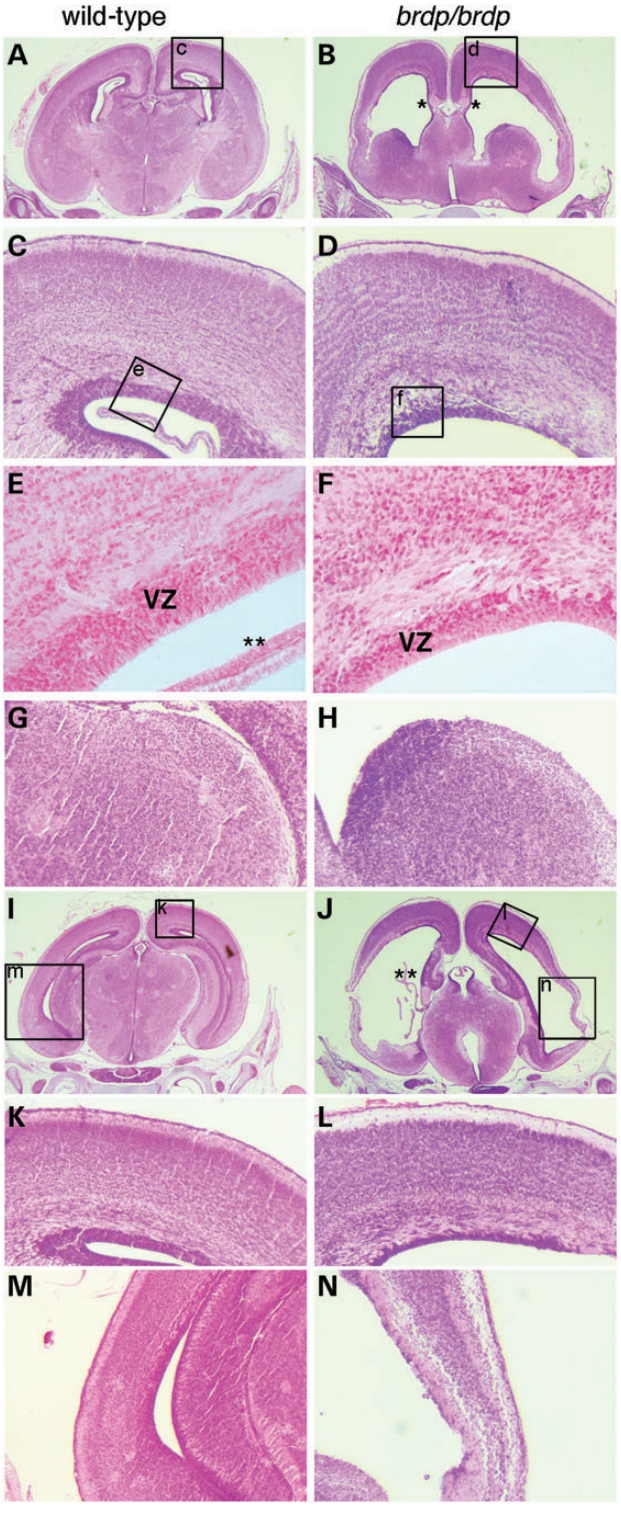

Figure 2. Histological analysis of brdp/brdp phenotype. (**A**–**H**) *Brdp/brdp* phenotypes at E18.5 include cortical thinning, loss of striatal tissue and agenesis of the CC (Probst bundles indicated by asterisks; B). A higher magnification view shows wave-like perturbations in the cortical plate (D), a smaller, irregular VZ (D and F) and the loss of striatal tissue (H). (**I**–**N**) Sections from more posterior regions of the brain show a more severe phenotype (compare B and J) with the dramatic thinning of the neuroepithelium especially pronounced in the area of the rhinencephalon (J and N) (VZ, ventricular zone; the double asterisk in E and J indicates the choroid plexus).

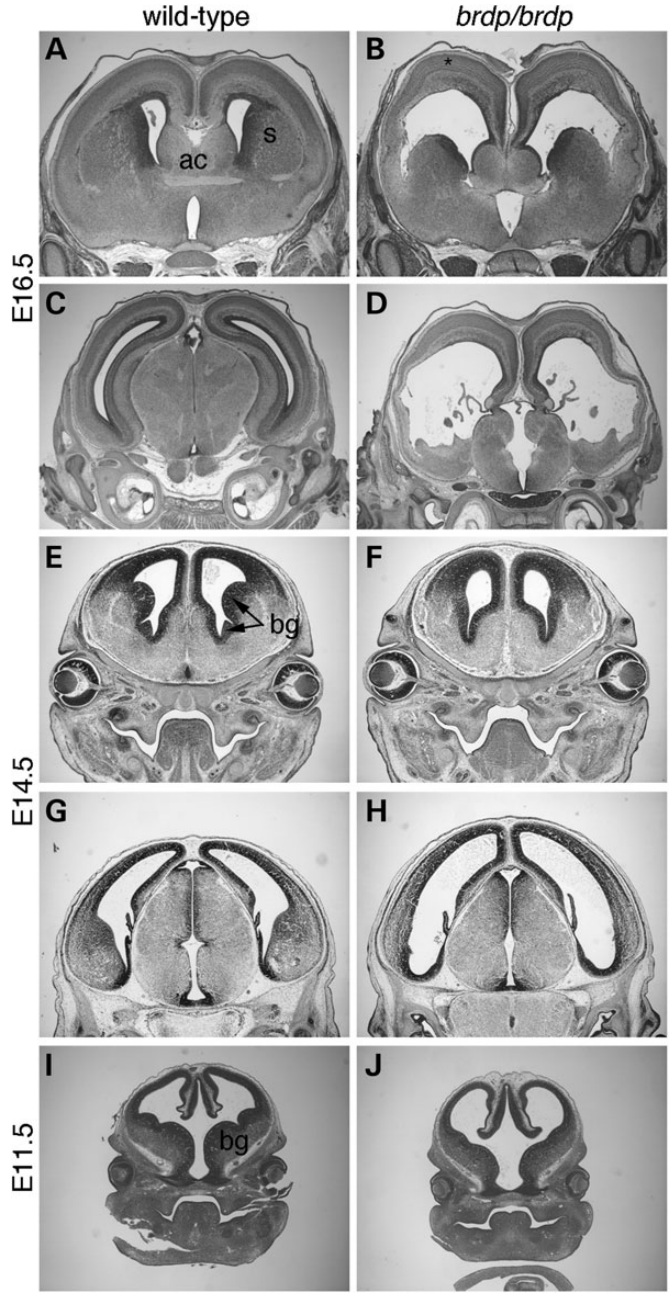

Figure 3. Brdp defects are visible throughout cortical development. (**A**–**D**) *Brdp/brdp* phenotypes including cortical thinning, loss of striatal tissue, agenesis of the CC and anterior commissure are evident by E16.5 in the anterior forebrain (B). Similar to perinatal stages, the *brdp* defect increases in severity in more posterior regions (D). At E14.5 (**E**–**H**), the loss of basal ganglionic structures is already evident throughout the anterior–posterior axis (E and F anterior to G and H). (**I** and **J**) At E11.5, the onset of neurogenesis, the *brdp* forebrain looks largely normal, suggesting that initial pattering is correct (ac, anterior commissure; bg, basal ganglia; s, striatum).

and cortical phenotypes, we performed immunohistochemistry for RC2, a marker of radial glial cells (Fig. 4L and M). Neither the phospho-vimentin nor the RC2 immunoreactivity patterns showed any signs of a morphological defect in the radial glial cells.

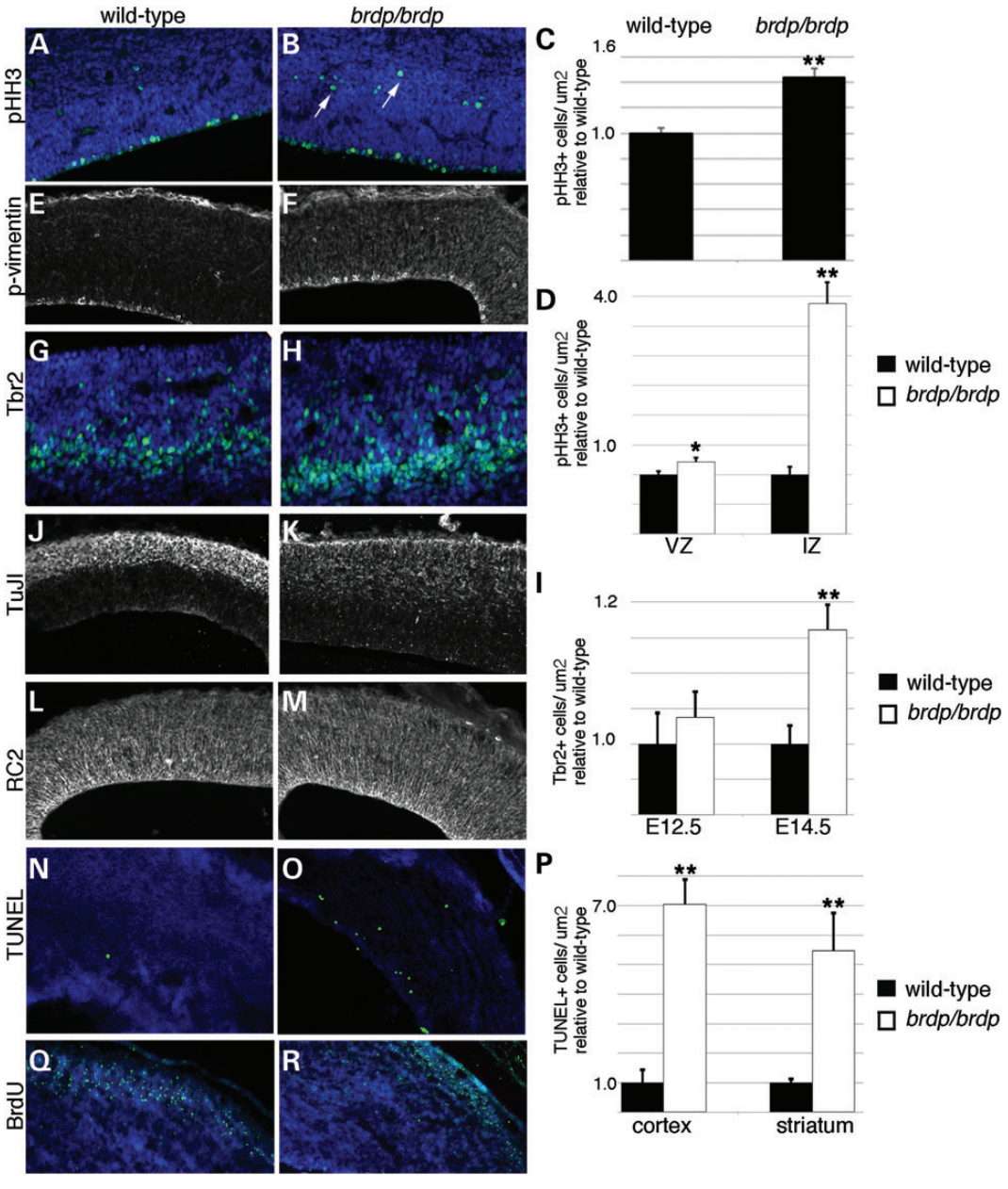

Figure 4. Molecular analysis of cortical development in brdp/brdp mutants reveals multiple defects. (**A**–**D**) The number of mitotic cells measured with pHH3 is increased in mutants at E14.5. We also note a significant increase in pHH3-positive cells in the intermediate zone (IZ; arrows in B). (**E** and **F**) Phospho-vimentin staining is also increased in mutants. (**G**–**I**) Tbr2 immunopositive cells are increased in mutants at E14.5. (**J** and **K**) Neuronal differentiation as marked by TuJI (E14.5) expression is reduced in mutants. Radial glial cells look morphologically normal in mutants (**L** and **M**). (**N**–**P**) Cell death is increased in the mutant cortex at E18.5 (N and O) and in both the striatum and the cortex at E16.5 (P). (**Q** and **R**) Neurons labeled with BrdU at E14.5 are able to migrate to the outer cortical plate by E18.5 in both mutant and wild-type. All data are graphed as a normalization to wild-type ± SEM. $^{*}P < 0.01$, $^{**}P < 0.001$.

Our observation in the mutants of an increase in proliferation but a reduced cortical plate suggests that neurons are not properly surviving. We measured the levels of cell death at multiple stages with the TUNEL (terminal deoxynucleotidyl transferase dUTP nick end labeling) assay and observed increases in mutant tissues when compared with wild-type mirroring the loss of tissue seen histologically (Fig. 4N–P). At E14.5, apoptosis in the cortex (13% increase in mutant, $P = 0.59$) and striatum (49% increase in mutant, $P = 0.16$) was increased only slightly when compared with control. At E16.5, however, we see significant increases in cell death in both the cortex (703% increase in mutant, $P < 0.0001$; Fig. 4P) and striatum (455% increase over wild-type, $P < 0.002$; Fig. 4P). Levels of cortical apoptosis were similarly increased at E18.5 (245% increase in mutant, $P < 0.015$).

Finally, we looked at migration of the neurons that do survive in the *brdp/brdp* mutants with a BrdU pulse-chase analysis. We labeled dividing neuron precursors at E14.5 and observed their location within the cortex at E18.5 (Fig. 4Q and R) with immunohistochemistry. We note that the majority of BrdU-positive

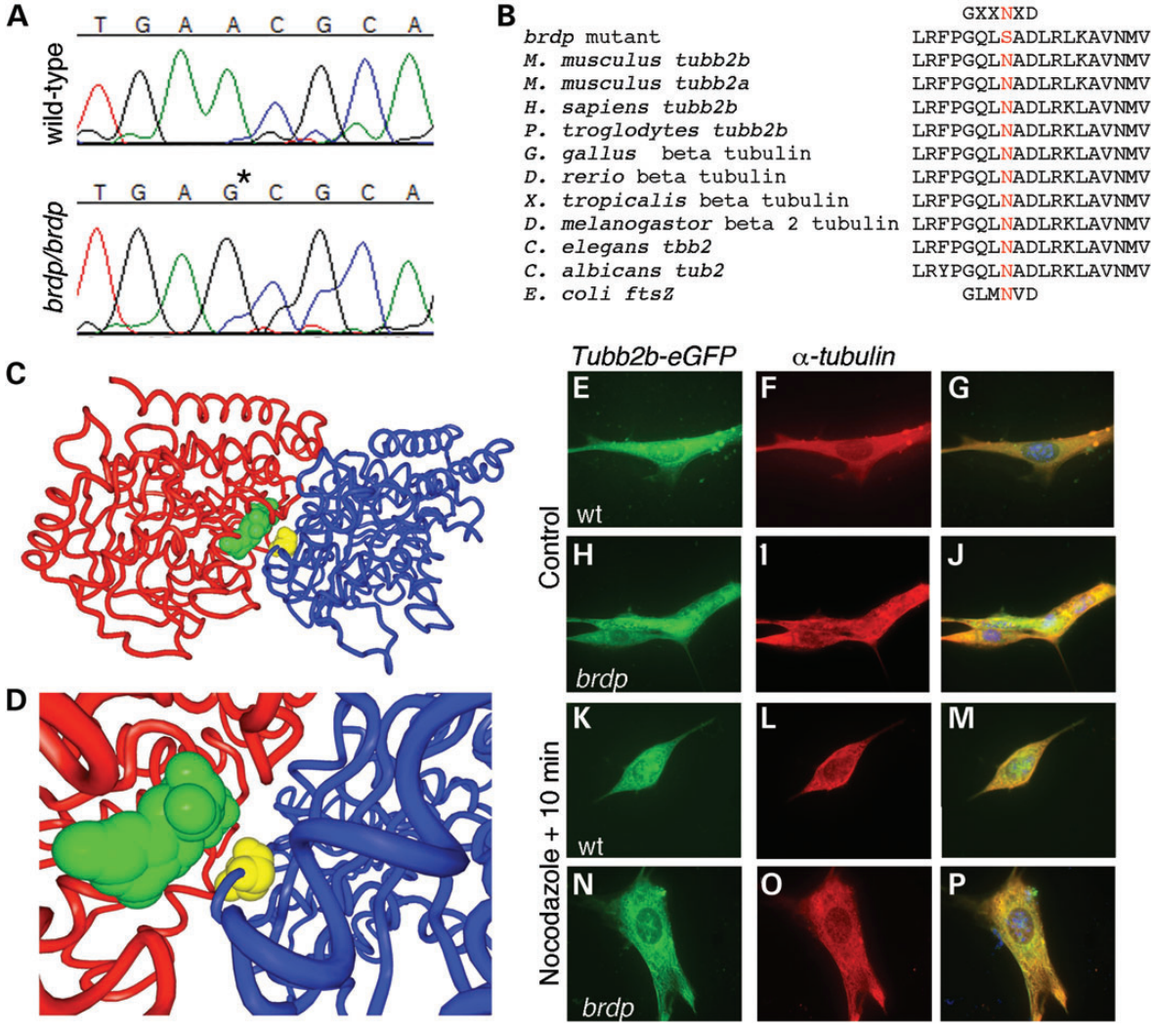

Figure 5. Tubb2b is the gene mutated in *brdp* mutants. (**A**) Sequencing of the *Tubb2b* locus identified a single-nucleotide change (indicated by an asterisk in *brdp/brdp* mutants resulting in a coding change from an asparagine residue to serine). (**B**) This N247S mutation is in a hyper-conserved region of the β-tubulin gene family: a GxxNxD domain conserved in all species examined. (**C**) The structure of the assembled α-tubulin (red structure) and β-tubulin (blue structure) subunits with the N247 residue of the β-subunit shown in yellow and the non-hydrolyzed GTP in green (pdb:1JFF). (**D**) More detailed view of the residue mutated in *brdp* mutants. (**E**–**P**) Transfection of wild-type *Tubb2b*-eGFP (E–G, K–M) or a *Tubb2b*^{brdp}-eGFP (H–J, N–P) into NIH3T3 cells followed by immunostaining for α-tubulin shows that both wild-type *Tubb2b*-eGFP and mutant *Tubb2b*^{brdp}-eGFP can incorporate into microtubular networks. (K–P) The microtubule network was depolymerized by nocodazole treatment and after a 10 min recovery; both wild-type and mutant monomers are incorporated into actively growing microtubules.

cells at this stage are found in the outer regions of the cortex in both wild-type and *brdp/brdp* mutants. We conclude from this that radial migration of surviving cortical neurons in the *brdp/brdp* mutants is not significantly compromised and the primary defect leading to a reduced cortical plate is the massive and sustained increase in apoptosis.

Tubb2b is the gene mutated in brdp mutants

We identified the causal gene in the *brdp* mutants with a positional cloning approach. An initial whole-genome single-nucleotide polymorphism (SNP) analysis performed on three affected mice localized the ENU mutation to a 30 Mb region on chromosome 13. Further genetic mapping resolved the recombinant interval to 4.7 Mb between SNPs rs29904172 and rs6259014. Four candidate genes in this region were identified and their coding regions were sequenced. We found no mutations in three other candidate genes and one mutation in the *Tubb2b* gene. An adenine-to-guanine single-nucleotide mutation results in the coding change of asparagine at residue 247 to serine (Fig. 5A). Quantitative RT–PCR indicated no significant differences in the expression of *Tubb2b* in mutant tissue compared with wild-type controls (data not shown). *Tubb2b* is very highly conserved across all species, and the N247S mutation is in a GxxNxD motif that is exquisitely conserved across phylogeny as far as the prokaryotic precursor to tubulin molecules, ftsZ (Fig. 5B; Supplementary Material, Fig. S2).

Tubulin polymers form by the assembly of alternating α and β monomeric subunits into tubulin protofilaments. We mapped the *brdp* mutation onto the structure of β-tubulin and found that the mutated residue is at the interface between the α- and β-subunits and the intradimeric, non-hydrolyzable GTP molecule (Fig. 5C

and D; Supplementary Material, Fig. S2). Mutations coding for alternative amino acids in this location would be consistent with defects in proper regulation of tubulin subunit assembly into functional protofilaments.

To further understand how this mutation might affect microtubule formation and function, we transfected NIH3T3 cells with a full-length *Tubb2b*-eGFP construct and a mutant construct where we recapitulated the *brdp* mutation in the plasmid sequence to express *Tubb2b*^{brdp}*-eGFP*. We fixed the cells and used immunocytochemistry for α-tubulin to highlight the microtubular network. In both cells transfected with the wild-type *Tubb2b*-eGFP, and the mutant *Tubb2b*^{brdp}*-eGFP* form, we note extensive colocalization of the α-tubulin and GFP-tagged β-tubulin subunits (Fig. 5E–J). We further tested the utility of the *Tubb2b*^{brdp}*-eGFP* tubulin monomers by treating the cells with nocodazole to depolymerize the microtubular network and assessing the ability of the mutant monomers to incorporate into rapidly reforming microtubules. Both wild-type and mutant constructs were able to incorporate into the reforming microtubular network (Fig 5K–P). We never noted any abnormal accumulation of tubulin monomers or reduced microtubule formation in any of these experiments. We conclude from these experiments that the *brdp* mutation does not completely block mutant forms of the TUBB2B protein from inclusion in forming microtubules, but may be deficient in more subtle aspects of microtubule form or function.

Brdp heterozygous mice have behavior and cortical patterning phenotypes

Routine animal husbandry revealed that the adult mice heterozygous for the *brdp* mutation displayed hyperactive behavior. We performed an open field test to more precisely measure this. Six animals of each genotype were placed in an open field and electronically monitored for 30 min. *Brdp/+* heterozygous animals covered a longer distance at a higher average speed than wild-type mice (271% of wild-type, $P = 0.006$, Fig. 6A). Heterozygous mice also entered each quadrant of the open field more often than wild-type mice (298% of wild-type, $P = 0.023$, Fig. 6B). These tests confirmed that *brdp* heterozygosity at the *tubb2b* locus leads to changes in behavior.

Given the profound cortical developmental defect in homozygous *brdp/brdp* mice and the behavioral phenotype in heterozygous *brdp/+* mice, we performed a molecular analysis of the adult *brdp/+* mice for possible cortical defects. RNA *in situ* hybridization for *T-box brain gene 1* (*Tbr1*) as a general marker for differentiated neurons showed weaker staining in the upper portion of the heterozygous cortex, but no significant decrease in the absolute number of expressing cells upon quantification (Fig. 7A). We next analyzed layer-specific cortical neuronal gene expression with four other markers. *Poliovirus receptor-related 3* (*Pvrl3*) in layer II/III was expressed at slightly reduced levels, and in a more diffuse pattern, in heterozygotes, but we did not see a significant decrease in the absolute number of cells expressing the gene (Fig. 7B). Markers of other layers did not show differences between heterozygotes and wild-type, including *RAR-related orphan receptor beta* in layer IV (*Rorb*, Fig. 7C), *Fez family zinc finger 2* in layer V (*Fezf2*, Fig. 7D) and *forkhead box P2* in layer VI (*Foxp2*, Fig. 7E). We did, however, see a significant decrease in *Gad1* (*glutamic acid decarboxylase 1*, also known as *Gad67*) expressing interneurons in the *brdp/+* heterozygotes when compared with littermates (89% of wild-type, $P = 0.037$; Fig. 7F). We further explored this interneuron deficit with immunohistochemistry for parvalbumin, somatostatin and calretinin as markers of a subset of the cortical, *Gad1*-positive interneurons (18) but saw no significant difference in cell numbers of any specific cell types between wild-type and *brdp/+* heterozygous mice (Supplementary Material, Fig. S3).

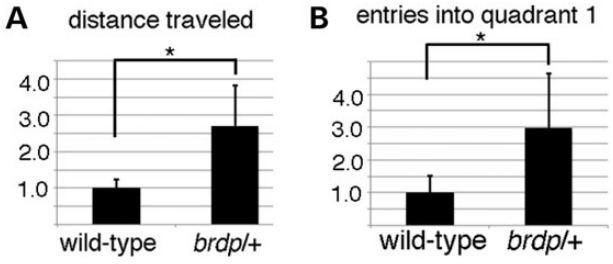

Figure 6. Brdp heterozygous mice are hyperactive. Wild-type and *brdp/+* heterozygous mice ($n = 6$ for each class) were measured in an open field for 30 min. Heterozygotes covered more distance (**A**) and were more exploratory (**B**) than wild-type animals. Data are shown normalized to wild-type ± SEM.

We have also found the *brdp* heterozygous mice to have extremely low fecundity on two separate inbred backgrounds, perhaps as a consequence of this hyperactivity. We also addressed the possibility that this reduced inbred fecundity may be a result of abnormal spermatogonial development given the expression of *Tubb2b* in the testis (19). A histological analysis of the testes from wild-type and *brdp/+* heterozygous males showed no difference in the length or density of spermatid tails in the developing testes (Supplementary Material, Fig. S4). We conclude that spermatid formation is not grossly affected, but sperm motility may be decreased in heterozygous males. Subsequent husbandry on the generally more fertile ICR/CD-1 outbred background has significantly mitigated this reduced fecundity observed on inbred backgrounds without affecting the forebrain phenotype.

DISCUSSION

In this report, we describe our cloning of the *brdp* mouse mutation as a missense mutation in the mouse *Tubb2b* gene. We describe behavioral phenotypes in the heterozygous mice. The homozygous *brdp/brdp* mutants are perinatal lethal and have a profoundly affected brain with significant cortical thinning, likely due to massively increased cell death. This finding in the homozygous *brdp* mice is the most dramatic neurodevelopmental phenotype identified to date in the mouse tubulin gene family. The *brdp* mutation represents a potential model of human cortical malformation and neurological disease as human TUBB2B heterozygous mutations result in polymicrogyria, neuronal migration defects and epilepsy (11).

The *brdp/brdp* homozygous mouse mutants are neonatal lethal and have a profoundly dysmorphic brain with a reduced neuroepithelium and ventriculomegaly. We have shown mitosis is actually increased in the mutant epithelium. Surprisingly, we also note an increase in mitotic cells in the region of the cortex, giving rise to the Tbr2-positive basal progenitors and a concomitant increase in Tbr2-positive cells themselves.

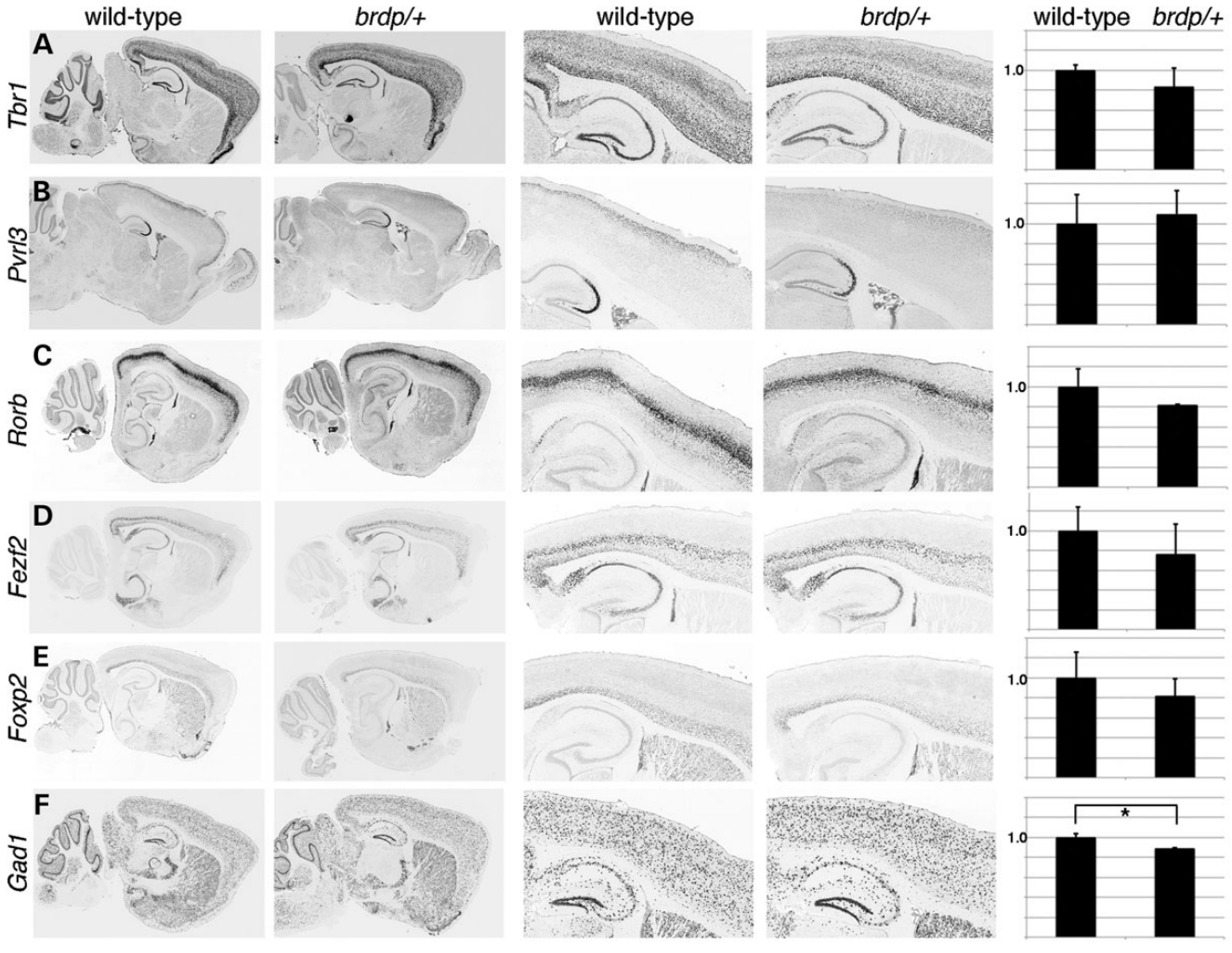

Figure 7. Brdp heterozygous mice have cortical defects. RNA *in situ* hybridization for multiple markers of cortical development shows subtle defects in the *brdp/+* heterozygous cortex. Each experiment was quantified as shown. Data are presented as the number of cells expressing the marker/ImageJ area, normalized to the wild-type average + SEM. Expression is shown for *Tbr1* (**A**), *Pvrl3* (**B**), *Rorb* (**C**), *Fezf2* (**D**), *Foxp2* (**E**) and *Gad1* (**F**). No significant difference was seen in the number of expressing cells for any gene except *Gad1*, which shows an 11% decrease in heterozygous compared with wild-type ($P = 0.037$). *Pvrl3* is not expressed in significantly fewer cells but is expressed at generally lower levels and over a broader portion of the cortex.

However, this is more than compensated for by a massive increase in cell death (~700% in the mutant cortex at E16.5). A particularly intriguing aspect of this phenotype is that the cortical thinning is much more dramatic in the lateral and posterior regions of the E18.5 forebrain. We note that cortical radial migration seems to be largely normal in homozygous mutants. Although most of our analysis focused on the cortex, we see an increase in cell death and developmental defects in the developing ganglionic eminences as well. Given these regions facilitate embryonic cortical development and are the inhibitory cells in the mature cortical circuitry, a contribution of these regions to the phenotypes in both the homozygous embryos and heterozygous adults cannot be discounted. The expression of *Tubb2b* is not reported to vary among different brain regions (11), perhaps suggesting that the regional nature of the *brdp* phenotype is due to partial compensation by another gene(s). Indeed, the closely related *Tubb2a* gene is physically adjacent to *Tubb2b* in the genome. *Tubb2a* is largely unstudied, but robust expression in the brain has been described (20,21).

The homozygous *brdp/brdp* phenotype does not appear to phenocopy an RNAi knockdown in the rat (11). We do not see evidence for a radial migration phenotype in our mice, whereas the RNAi knockdown clones do show a migration defect. It is of note that cell death was not directly assayed in the knockdown migration experiments. Although there may be differences due to experimental design, we conclude that the *brdp* allele may not be a null allele because of the discrepancy with the RNAi phenotype. Rather, the homozygous missense mutation may alter microtubule function in a manner that results in decreased cell survival rather than migration. A true null allele would be a useful tool to further query this hypothesis as well as address the larger multi-tubulin hypothesis.

We also report phenotypes in the *brdp/+* heterozygous adult mutant mouse somewhat similar to those seen in the human TUBB2B patients (11). Human patients have been noted with epilepsy and polymicrogyria, suggestive of neuronal migration defects. We see behavioral defects in the heterozygous mice with a concomitant decrease in the number of interneurons

expressing high levels of *Gad1*. This possible reduction of interneuron modulation of cortical activity is consistent with the behavioral phenotypes we see in the mouse and the epilepsy in humans. However, we do not note a reduction in the number of any specific interneuron cell type as assayed by immunohistochemistry with parvalbumin, somatostatin or calretinin. These findings are somewhat discordant and this may be because the measure of *Gad1* activity was via RNA *in situ* hybridization and quantifying the number of cells that exceeded an expression threshold. In contrast, the interneuron cell-type-specific assays used fluorescent immunohistochemistry. Other than the interneuron deficit, the *brdp*/+ cortex appears to be largely normal although we do note the upper layer neuronal marker *Pvrl3* is expressed across a broader area of the cortex and is expressed at slightly reduced levels as measured by RNA *in situ* hybridization.

The *brdp*/+ phenotype has features reminiscent of other mouse tubulin alleles. Both *brdp*/+ and *Tuba1*/+ heterozygous mice have cortical lamination defects, are hyperactive and present difficulties in breeding. *Tuba1*/+ mice were reportedly not able to be intercrossed at all (2). *Tuba1* mice were also reported to have wave-like perturbations of cortical layering similar to what we see in the *brdp* homozygotes, although this was not visualized using layer-specific marker analysis. The *Tubb3*$^{R262C/R262C}$ mice had some of the axon tract phenotypes we observed in *brdp* mice, namely in the CC and anterior commissure (9). These studies taken together with our findings continue to support the idea of an overlapping spectrum of phenotypes due to tubulin mutations.

The precise molecular function of *Tubb2b* in cortical development is still unclear. Our analysis suggests that the amino acid substitution in the *brdp* allele is in the region of contact between the α- and β-subunits of the microtubule polymer. We do, however, note that the expression of β-tubulin constructs with the *brdp* mutation still results in the incorporation of 'mutant' monomers into polymerizing microtubules, indicating that this mutation does not completely block multimer formation. This has been observed when other mutations in human tubulin genes leading to neural phenotypes are modeled in these assays (2,11). Indeed, to date, there is no correlation between the severity of mutation and the location of the affected residue on the structure of the tubulin monomer. The location of the mutated amino acid in the *brdp* mutant suggests that it may affect the stability of the protofilaments, rather than tubulin dimer interaction(s) with a microtubule-associated protein (Fig. 5). The most striking phenotype in our mice is the increase in intermediate progenitor division and apoptosis. How a mutation in *Tubb2b* might lead to these phenotypes will require further study.

Further study of *Tubb2b* is necessary to generate a more complete mechanistic understanding of the role of *Tubb2b* in the developing cortex. The *brdp* mutation results in exceedingly low fecundity in two inbred backgrounds. We have since outcrossed to the CD-1 background and seen a dramatic increase in fecundity without a loss of the *brdp* phenotype, which will expedite future studies of *Tubb2b*. Creation of a conditional allele would be an especially useful reagent to further explore the precise mechanism leading to the *brdp* phenotype, especially in postnatal neural development. The adult expression of *Tubb2b* is reported to be much more limited than the expression at embryonic stages [e.g. cerebellar Purkinje cells and hippocampal cells (11), and the role of *Tubb2b* in these structures could also be studied in a conditional deletion].

MATERIALS AND METHODS

Mouse husbandry

Animals were initially maintained as a mixed A/J, FVB stock. The allele was isolated in an ENU mutagenesis experiment in which A/J males were mutagenized and outcrossed to FVB females (16). Upon isolation of the *brdp* mutation, the colony was initially maintained by a combination of intercross and outcross to FVB. Matings were monitored and noon of the day of copulation plug was determined to be E0.5. Routine genotyping was performed with a flanking RFLP marker at ch13:34.2 Mb (F primer: CACAACTGTCTTTAGAGGATGTGAA; R primer GCAGAACACATTGTCGTCTTGT followed by *Mse*I digestion) and ch13:33.5 (F primer: TCAATGCTGCCAATT TTTCA; R primer TCCTCCCTCCTTACCCAA followed by *Bbs*I digestion) and primers amplifying SNPs polymorphic between the AJ and FVB strains. All animals were maintained in accordance with HMS and CCHMC IACUC guidelines. The *brdp* allele was also outcrossed to C57BL6/J (Jackson Labs) and CD-1 (Charles River) mice. Genotyping on the B6 background was done with the ch13:34.2 marker. The *brdp* mutation also creates a *Blp*I restriction site (F primer: ACAAAGGGTG-GAGGAGTGTG; R primer: TTGGAGTCGAACATCTGCTG) and this was used for genotyping mice on the CD1 background.

Genetic mapping

The mapping of the *brdp* mutant has been described (17). Briefly, an initial genome scan was done with multiple mutant embryos using a 768 marker whole-genome SNP panel to identify a region of shared A/J homozygosity among mutants, similar to a method described previously (22). After the identification of the candidate region, exon-directed sequencing of four genes in the interval ultimately revealed the *brdp* mutation in *Tubb2b*.

Histology and *in situ* hybridization

Samples for histological analysis were fixed in Bouin's fixative, prepared using a Leica TP1020 automated tissue processor, sectioned at 14 μm and stained using established protocols. All paired images presented are of equal magnification. For qPCR analysis, total RNA from embryos was prepared with the TRIZOL reagent, and cDNA was prepared with the qScript cDNA supermix (Quanta). PCR analysis was with Perfecta SYBR Green Supermix (Quanta) and performed on a Bio-Rad iCycler. Primers were: Tubb2b-F (TGAGCATGGTATA-GACCCCAC), Tubb2b-R (ACCTGACTGAGTCCATTG TGC), Gapdh-F (ACTCCACTCACGGCAAATTC) and Gapdh-R (TCTCCATGGTGGTGAAGACA). Nissl staining and section *in situ* hybridization was done at the Allen Institute for Brain Science as previously described (21).

Cell death analysis

Pregnant dams were harvested at E14.5, E16.5 and E18.5. Embryos were fixed in 4% paraformaldehyde, embedded for

cryopreservation and sectioned at 14 μm. Samples were prepared using the Click-iT® TUNEL Alexa-Fluor® 488 Imaging Assay kit (C10245, Invitrogen/Life Technologies). The manufacturer's protocol was followed with the exception of permeabilizing, but not fixing, the embedded tissues. Sections were stained with DAPI to visualize cell nuclei and slides were mounted in ProLong AntiFade (Invitrogen) and sealed. Microscopy was performed on a Zeiss AxioImager and cell count analysis was completed using the IMARIS 7.5.1 software or NIH ImageJ.

BrdU labeling

Pregnant dams were injected i.p. with 20 μl per 10 g mouse weight of a 10 mg/ml BrdU (Sigma) solution on E14.5 and sacrificed on E18.5. Cryosections were cut at 14 μm and BrdU immunohistochemistry was performed with standard protocols. In brief, sections were washed with PBS followed by antigen retrieval using citrate buffer and 2N HCl. Slides were blocked with 5% NGS-PBST for 1 h at room temperature and then incubated with the Rat-BrdU antibody (Abcam; 1:40) in 5% NGS-PBST overnight at 4°C. Sections were washed and incubated with Alexa-Fluor488 goat anti-rat (Invitrogen, 1:500) for 1 h at room temperature. Sections were stained, mounted, imaged and quantified as described earlier.

Immunohistochemistry

Both cryosections and paraffin sections were used for immunohistochemistry. In both cases, antigen retrieval was performed with an antigen unmasking solution (Vector Laboratories). Sections were blocked with 5% normal goat serum/PBST and primary antibodies were incubated overnight. Primary antibodies used in this study were anti-pHH3 (Sigma, 1:500), phospho-vimentin (Abcam, 1:1000), Tbr2 (Abcam, 1:500), TuJI (Sigma, 1:500), RC2 (DSHB, 1:10), parvalbumin (SWANT, 1:5000), somatostatin (Abcam, 1:500) and calretinin (Abcam, 1:500). Sections were rinsed with PBST and incubated with an Alexa-Fluor 594 goat anti-rabbit secondary antibody (Molecular Probes, 1:500) for 1 h at room temperature. Sections were stained, mounted, imaged and quantified as described earlier. All paired images are shown at identical magnification.

Quantification of immunohistochemistry

Quantification of mitotic cells was performed by counting fields of cells parallel to the VZ with Imaris 7.5.1. Cells immunoreactive for pHH3 were counted as a proportion of all cells in the field (DAPI-positive), and a mitotic index was generated. Measurements of TUNEL-positive cells, total cell number and interneuron immunoreactivity in *brdp*/+ adults were done similarly. In order to quantify *brdp*/+ *in situ* hybridization results, high-resolution images of data generated at the Allen Brain Institute were analyzed with the ImageJ software. The area of the cortex was defined and cells with an *in situ* signal above a standard threshold were normalized to the cortical area. All statistical analyses were performed in Excel.

Cell culture, transfections and immunofluorescence

NIH 3T3 cells were cultured in DMEM medium (Gibco) supplemented with 10% fetal bovine serum and 1% Pen/Strep at 37°C, 5% CO_2. Cells were plated on 0.2% gelatin-coated coverslips to reach a maximum density of 5000 cells/0.32 cm^2 plate area on the day of nocodazole treatment. Cells were transfected with the pCMV-AC-GFP vector expressing either wild-type *Tubb2b* sequence or a *Tubb2b*^{brdp} construct generated by site-directed mutagenesis (Stratagene). Transfections were performed with FUGENE (Promega) as per the manufacturer's instructions (3:2 ratio of the FUGENE/DNA). For nocodazole treatment, cells were treated with 5 μM nocodazole for 15 min and washed. Cells were fixed with 0.5 ml of cold 100% methanol at −20°C for 3 min. Permeabilization was achieved by a 10 min treatment with 0.1% Triton X-100/PBS prior to methanol fixation. Cells were stained using standard protocols for α-tubulin (Sigma clone DM1A, 1:1500 in 1% BSA) with an Alexa-Fluor 594 goat anti-mouse secondary (1:1500, Invitrogen) antibody.

Structural modeling

The structure of a tubulin sheet stabilized with taxol was identified in the RCSB protein data bank (http://www.pdb.org/pdb/home/home.do; structure 1JFF) and analyzed using the GRASP2 software (23).

Open-field testing

Six wild-type and six heterozygous female mice aged 8–10 weeks were tested. Naïve animals were placed in a square enclosure and their movement was tracked with video equipment for 30 min. Animal movement was analyzed with the VideoMot2 video tracking system (TSE systems). The following parameters were recorded: total distance traveled, average speed and entries into one portion of the enclosure (termed quadrant 1).

SUPPLEMENTARY MATERIAL

Supplementary Material is available at *HMG* online.

ACKNOWLEDGEMENTS

We thank T. Siggers for help with the structural modeling in Figure 3, M. Koffron for assistance with the Imaris software, A. Wynshaw-Boris for discussion of these data and C. Walsh and members of the Stottmann laboratory for comments on the manuscript. The RC2 monoclonal antibody developed by M. Yamamoto was obtained from the Developmental Studies Hybridoma Bank developed under the auspices of the NICHD and maintained by the Department of Biology, The University of Iowa, Iowa City, IA 52242, USA.

Conflict of Interest statement. D.A.S. is a consultant to GlaxoSmithKline and Genocea, a vaccine company.

FUNDING

This work was supported by the National Institutes of Health (grant numbers HD36404, MH081187 to D.R.B., HD053198 to R.W.S. and AG027916 to D.A.S.) and laboratory start-up funds from the Cincinnati Children's Hospital Research Foundation (R.W.S.).

REFERENCES

1. Tischfield, M.A., Cederquist, G.Y., Gupta, M.L. Jr and Engle, E.C. (2011) Phenotypic spectrum of the tubulin-related disorders and functional implications of disease-causing mutations. *Curr. Opin. Genet. Dev.*, 10.1016/j.gde.2011.01.003.
2. Keays, D.A., Tian, G., Poirier, K., Huang, G.-J., Siebold, C., Cleak, J., Oliver, P.L., Fray, M., Harvey, R.J., Molnár, Z. *et al.* (2007) Mutations in α-tubulin cause abnormal neuronal migration in mice and lissencephaly in humans. *Cell*, **128**, 45–57.
3. Poirier, K., Keays, D.A., Francis, F., Saillour, Y., Bahi, N., Manouvrier, S., Fallet-Bianco, C., Pasquier, L., Toutain, A., Tuy, F.P.D. *et al.* (2007) Large spectrum of lissencephaly and pachygyria phenotypes resulting from de novo missense mutations in tubulin alpha 1A (TUBA1A). *Hum. Mutat.*, **28**, 1055–1064.
4. Morris, R.D.J., Najm, J., Lachmeijer, A.M.A., Sztriha, L., Martins, M., Kuechler, A., Haug, V., Zeschnigk, C., Martin, P., Santos, M. *et al.* (2008) Refining the phenotype of alpha-1a tubulin (TUBA1A) mutation in patients with classical lissencephaly. *Clin. Genet.*, **74**, 425–433.
5. Bahi-Buisson, N., Poirier, K., Boddaert, N., Saillour, Y., Castelnau, L., Philip, N., Buyse, G., Villard, L., Joriot, S., Marret, S. *et al.* (2008) Refinement of cortical dysgeneses spectrum associated with TUBA1A mutations. *J. Med. Genet.*, **45**, 647–653.
6. Cushion, T.D., Dobyns, W.B., Mullins, J.G.L., Stoodley, N., Chung, S.K., Fry, A.E., Hehr, U., Gunny, R., Aylsworth, A.S., Prabhakar, P. *et al.* (2013) Overlapping cortical malformations and mutations in TUBB2B and TUBA1A. *Brain*, 10.1093/brain/aws338.
7. Jansen, A.C., Oostra, A., Desprechins, B., De Vlaeminck, Y., Verhelst, H., Régal, L., Verloo, P., Bockaert, N., Keymolen, K., Seneca, S. *et al.* (2011) TUBA1A mutations: from isolated lissencephaly to familial polymicrogyria. *Neurology*, **76**, 988–992.
8. Abdollahi, M.R., Morrison, E., Sirey, T., Molnár, Z., Hayward, B.E., Carr, I.M., Springell, K., Woods, C.G., Ahmed, M., Hattingh, L. *et al.* (2009) Mutation of the variant alpha-tubulin TUBA8 results in polymicrogyria with optic nerve hypoplasia. *Am. J. Hum. Genet.*, **85**, 737–744.
9. Tischfield, M.A., Baris, H.N., Wu, C., Rudolph, G., Van Maldergem, L., He, W., Chan, W.-M., Andrews, C., Demer, J.L., Robertson, R.L. *et al.* (2010) Human TUBB3 mutations perturb microtubule dynamics, kinesin interactions, and axon guidance. *Cell*, **140**, 74–87.
10. Poirier, K., Saillour, Y., Bahi-Buisson, N., Jaglin, X.H., Fallet-Bianco, C., Nabbout, R., Castelnau-Ptakhine, L., Roubertie, A., Attie-Bitach, T., Desguerre, I. *et al.* (2010) Mutations in the neuronal-tubulin subunit TUBB3 result in malformation of cortical development and neuronal migration defects. *Hum. Mol. Genet.*, **19**, 4462–4473.
11. Jaglin, X.H., Poirier, K., Saillour, Y., Buhler, E., Tian, G., Bahi-Buisson, N., Fallet-Bianco, C., Phan-Dinh-Tuy, F., Kong, X.P., Bomont, P. *et al.* (2009) Mutations in the β-tubulin gene TUBB2B result in asymmetrical polymicrogyria. *Nat. Genet.*, **41**, 746–752.
12. Cederquist, G.Y., Luchniak, A., Tischfield, M.A., Peeva, M., Song, Y., Menezes, M.P., Chan, W.M., Andrews, C., Chew, S., Jamieson, R.V. *et al.* (2012) An inherited TUBB2B mutation alters a kinesin-binding site and causes polymicrogyria, CFEOM and axon dysinnervation. *Hum. Mol. Genet.*, 10.1093/hmg/dds393.
13. Amrom, D., Tanyalçin, I., Verhelst, H., Deconinck, N., Brouhard, G., Décarie, J.-C., Vanderhasselt, T., Das, S., Hamdan, F., Lissens, W. *et al.* (2013) Polymicrogyria with dysmorphic basal ganglia? Think tubulin! *Clin. Genet.*, 10.1111/cge.12141.
14. Guerrini, R., Mei, D., Cordelli, D.M., Pucatti, D., Franzoni, E. and Parrini, E. (2012) Symmetric polymicrogyria and pachygyria associated with TUBB2B gene mutations. *Eur. J. Hum. Genet.*, **20**, 995–998.
15. Romaniello, R., Tonelli, A., Arrigoni, F., Baschirotto, C., Triulzi, F., Bresolin, N., Bassi, M.T. and Borgatti, R. (2012) A novel mutation in the β-tubulin gene TUBB2B associated with complex malformation of cortical development and deficits in axonal guidance. *Dev. Med. Child Neurol.*, **54**, 765–769.
16. Schwer, H.D., Lecine, P., Tiwari, S., Italiano, J.E., Hartwig, J.H. and Shivdasani, R.A. (2001) A lineage-restricted and divergent beta-tubulin isoform is essential for the biogenesis, structure and function of blood platelets. *Curr. Biol.*, **11**, 579–586.
17. Stottmann, R.W., Moran, J.L., Turbe-Doan, A., Driver, E., Kelley, M. and Beier, D.R. (2011) Focusing forward genetics: a tripartite ENU screen for neurodevelopmental mutations in the mouse. *Genetics*, **188**, 615–624.
18. Augood, S.J., Herbison, A.E. and Emson, P.C. (1995) Localization of GAT-1 GABA transporter mRNA in rat striatum: cellular coexpression with GAD67 mRNA, GAD67 immunoreactivity, and parvalbumin mRNA. *J. Neurosci.*, **15**, 865–874.
19. Braun, A., Breuss, M., Salzer, M.C., Flint, J., Cowan, N.J. and Keays, D. (2010) Tuba8 is expressed at low levels in the developing mouse and human brain. *Am. J. Hum. Genet.*, **86**, 819–822.
20. Leandro-García, L.J., Leskelä, S., Landa, I., Montero-Conde, C., López-Jiménez, E., Letón, R., Cascón, A., Robledo, M. and Rodríguez-Antona, C. (2010) Tumoral and tissue-specific expression of the major human beta-tubulin isotypes. *Cytoskeleton (Hoboken)*, **67**, 214–223.
21. Lein, E.S., Hawrylycz, M.J., Ao, N., Ayres, M., Bensinger, A., Bernard, A., Boe, A.F., Boguski, M.S., Brockway, K.S., Byrnes, E.J. *et al.* (2007) Genome-wide atlas of gene expression in the adult mouse brain. *Nature*, **445**, 168–176.
22. Moran, J.L. (2006) Utilization of a whole genome SNP panel for efficient genetic mapping in the mouse. *Genome Res.*, **16**, 436–440.
23. Petrey, D. and Honig, B. (2003) GRASP2: visualization, surface properties, and electrostatics of macromolecular structures and sequences. *Meth. Enzymol.*, **374**, 492–509.